

Evidence for strain-induced lateral carrier confinement in InGaAs quantum wells by low-temperature near-field spectroscopy

U. Zeimer,^{a)} F. Bugge, S. Gramlich, V. Smirnitcki, M. Weyers, and G. Tränkle
Ferdinand-Braun-Institut für Höchstfrequenztechnik, Albert-Einstein-Straße 11, D-12489 Berlin, Germany

J. Grenzer and U. Pietsch
Institut für Physik, Universität Potsdam, Am Neuen Palais 10, D-14415 Potsdam, Germany

G. Cassabois, V. Emiliani, and Ch. Lienau
Max-Born-Institut für nichtlineare Optik und Kurzzeitspektroskopie, Max-Born-Straße 2A, D-12489 Berlin, Germany

(Received 10 April 2001; accepted for publication 23 July 2001)

A strain-induced lateral variation of the band edges of a 10-nm-thick $\text{In}_{0.16}\text{Ga}_{0.84}\text{As}$ quantum well embedded in GaAs is achieved by patterning of a 100-nm-thick compressively strained $\text{In}_{0.52}\text{Ga}_{0.48}\text{P}$ stressor layer. The strain modulation results in a splitting of the 10 K far-field photoluminescence (PL) spectra into two emission peaks. Spectrally resolved two-dimensional near-field PL images establish a clear spatial and spectral separation of the two far-field PL peaks, indicating a lateral carrier confinement with a confinement energy of about 10 meV. Finite-element calculations of the strain distribution are used to determine the lateral band-edge shifts and are well in agreement with the experimental findings. © 2001 American Institute of Physics. [DOI: 10.1063/1.1402638]

It is well known that carrier confinement in two or three dimensions can improve the performance of semiconductor laser devices, i.e., a higher thermal stability and a higher modal gain can be achieved.^{1,2} Besides the confinement in the vertical (growth) direction, which is implemented by the layer sequence, several concepts have been used to create a lateral confinement. One important approach is to exploit self-organized growth of heavily strained three-dimensional (3D) islands of active material.³ In this case, device performance still suffers from the nonuniformity of the size and shape of the islands. Lateral confinement can also be established by etching through the quantum well and subsequent regrowth.⁴ The free surface or the regrown interface can, however, act as a source for nonradiative recombination centers, deteriorating the device properties.⁵ Kash and co-workers^{6,7} proposed to exploit a patterned stressor layer in order to introduce a lateral strain modulation into a buried single quantum well (SQW) for lateral band-structure engineering. In this design, the SQW itself remains unaffected by the etching procedure and nonradiative recombination centers can be avoided. While in their case the stressor layer material was hydrogenated carbon, a semiconductor stressor layer is desirable for device applications. Sopranen, Lipsanen, and Ahopelto⁸ used self-assembled InP islands on top of an InGaAs SQW to achieve a lateral strain modulation which modified the SQW photoluminescence (PL) spectra. However, the size of the dots can change, and thus the strain modulation can be inhomogeneous. Recently, we have shown⁹ that InGaP can successfully be used as a stressor for a 10-nm-thick $\text{In}_x\text{Ga}_{1-x}\text{As}$ SQW ($x=0.16$). The stressor pattern in our case consists of a surface grating which was prepared by holographic photolithography and subsequent

wet-chemical etching of the InGaP. For a particular strain status in the InGaP layer before patterning ($\epsilon = -0.3\%$), and a particular grating geometry, the strain distribution was calculated using elasticity theory in a finite-element method (FEM) approach. The FEM results were confirmed by x-ray diffraction measurements in grazing-incidence geometry (GID).

In this letter we demonstrate, using low-temperature near-field scanning optical microscopy (NSOM), that the strain-induced lateral band-gap variation in these samples results in spatially and spectrally distinct PL emission peaks, indicating a lateral carrier confinement with a confinement energy of about 10 meV.

The vertical layer sequence was grown by low-pressure metalorganic vapor-phase epitaxy at 650 °C in a horizontal Aix200 reactor on an exactly oriented 2 in. GaAs(001) substrate. As precursors, trimethylgallium, trimethylindium, arsine, and phosphine were used. The $\text{In}_{0.16}\text{Ga}_{0.84}\text{As}$ SQW ($\epsilon_{\text{II}} = -1.1\%$) with a thickness of 10 nm is sandwiched between a GaAs buffer layer and a 10-nm-thick GaAs layer, which serves as a barrier and etch-stop layer. The 120-nm-thick InGaP layer on top of it with a compressive strain of $\epsilon_{\text{II}} = -0.3\%$ is followed by a 10-nm-thick GaAs cap layer. The lateral surface grating with a period of 1 μm and a ridge/valley ratio of 2.7 was prepared as described in Ref. 9. The trapezoidal grating facets have nearly {111} orientation and the ridges and valleys run parallel to [1-10]. We have chosen a period of 1 μm to prevent lateral quantization effects and an overlap of the strain fields from adjacent valleys. In the valleys the InGaP was completely removed down to the GaAs etch-stop layer.

Far-field PL spectra (Fig. 1) were recorded at 10 K by using a HeNe laser with an incident power of 4 mW as the excitation source, focused down to a 0.2 mm spot. The bottom curve shows the PL spectrum from the sample before

^{a)}Author to whom correspondence should be addressed; electronic mail: zeimer@fbh-berlin.de

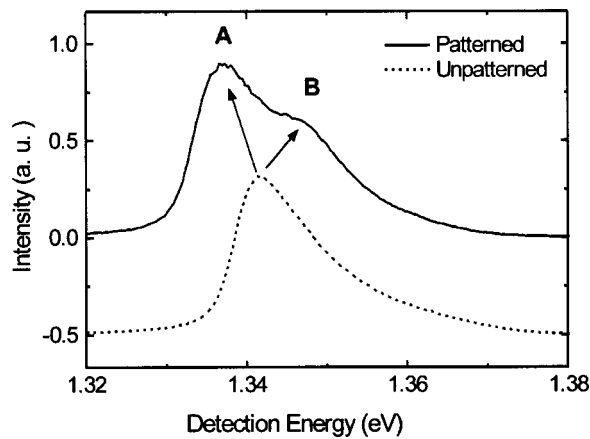


FIG. 1. 10 K far-field PL spectra of the as-grown sample (dashed line) and the patterned sample (solid line). The patterned sample shows two emission peaks, A and B, centered around 1.337 and 1.35 eV, respectively.

patterning, exhibiting a single emission peak at 1.342 eV, as expected for the In content of $x = 0.16$ in the SQW and a full width at half maximum (FWHM) of 10 meV. The asymmetric line shape is likely to result from fluctuations of the alloy composition of the InGaP at the nanometer length scale as identified by transmission electron microscopy. After patterning, two peaks are resolved (top curve), peak A at lower energy (1.337 eV) with higher intensity and peak B at higher energy (1.347 eV) with lower intensity.

To assign the microscopic origin of the two emission peaks, two-dimensional near-field PL images were recorded at 10 K with a home-built near-field microscope.¹⁰ The microscope is used in the illumination/collection geometry: The HeNe excitation laser (1.96 eV) is transmitted through an uncoated etched near-field fiber probe and PL is collected back through the same fiber. Local PL spectra are acquired at each tip position with an $f = 50$ cm monochromator in conjunction with a charge-coupled-device (CCD) camera while scanning the tip. In this geometry we achieve a combined spatial and spectral resolution of 150 nm and 100 μeV , respectively.¹¹ Shear-force images of the surface topography were recorded simultaneously with the near-field PL images and allowed us to correlate the optical image and sample topography with an accuracy better than 100 nm.

Figure 2(a) shows a two-dimensional near-field PL image detected at an emission energy E_{det} of 1.337 eV, i.e., the center of peak A in Fig. 1. In the image, the PL intensity is spectrally averaged at each tip position over a range of 2 meV. The tip is scanned across a $3 \times 2 \mu\text{m}^2$ area comprising three ridges and four valleys with a pixel of 60 nm. Comparing the near-field image to the simultaneously recorded surface topography (not shown), we find the maximum PL intensity exactly at the center of the ridge. The spectral distribution of the near-field PL at the ridge center, $A(E_{\text{det}})$, is shown in Fig. 2(d). It shows a single emission peak and is similar to that of the unpatterned quantum well (QW) but blueshifted by 5 meV to 1.338 eV. Near the valley center the near-field PL spectra are strikingly different. First, the emission intensity at $E_{\text{det}} = 1.338$ eV decreases to less than 40% of its maximum value at the ridge center. This is clearly seen in Fig. 2(c), open circles, showing a cross section through Fig. 2(a) along a line perpendicular to the ridges. In addition to

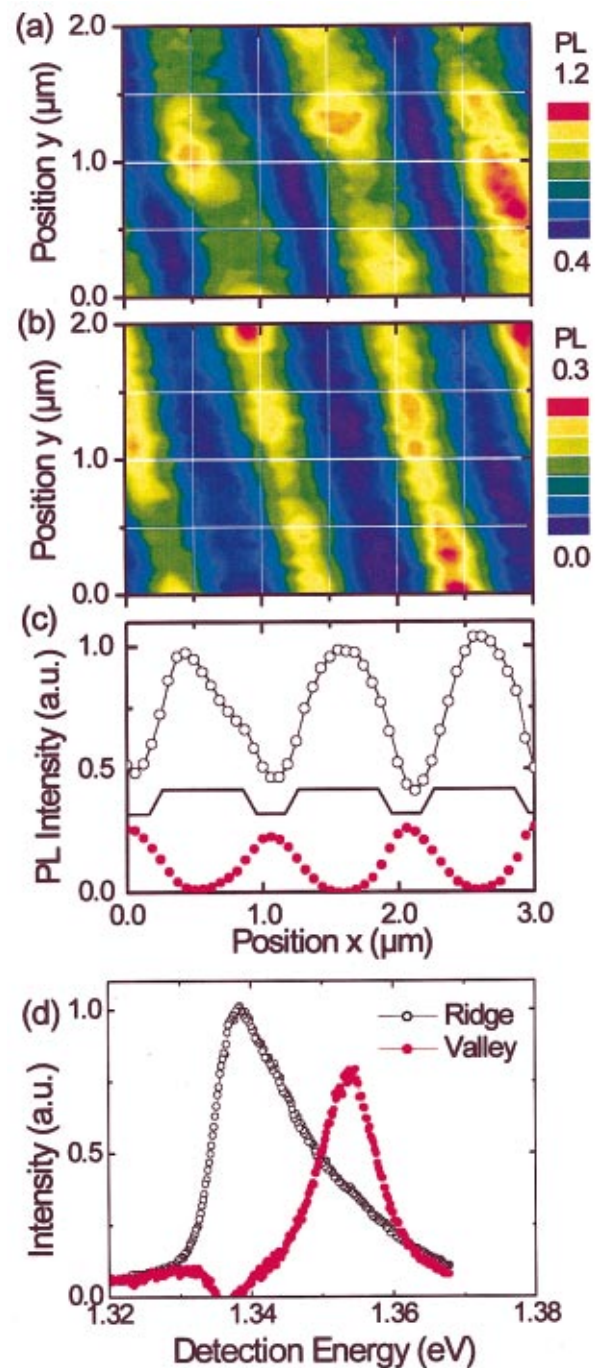


FIG. 2. (Color) (a) Two-dimensional image of the near-field PL intensity distribution in the range from 1.338 to 1.340 eV (peak A). High intensity is found under the grating ridges. (b) Two-dimensional image of the near-field PL intensity of transition B, detected in the range from 1.351 to 1.353 eV. High intensity is found in the grating valleys. (c) Cross sections through (a) and (b) showing line scans along the ridge direction of the PL intensity for transitions A (open circles) and B (filled circles) and highlighting the spatial anticorrelation between both emission components. A schematic of the ridge pattern is indicated. (d) 10 K near-field PL spectra of the patterned sample: PL spectrum of transition A, taken at the ridge center (open circles); PL spectrum of transition B, taken at the valley center (filled circles).

the transition $A(E_{\text{det}})$ we find a second emission component, transition B, that shows a narrower, Gaussian-like distribution $B(E_{\text{det}})$ centered at 1.353 eV with a FWHM of 10 meV [Fig. 2(d), filled circles]. The spatial distribution of this second emission component is spatially anticorrelated to that of transition A and the maximum of the PL intensity is found at

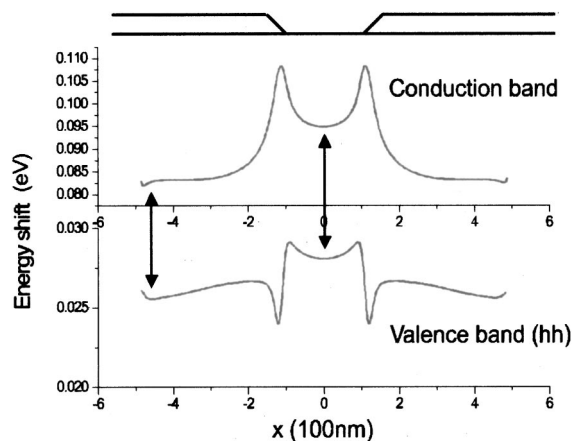


FIG. 3. Calculations of the conduction- (upper curve) and valence- (lower curve) band-edge shifts as a function of the lateral position along the grating repetition direction using deformation potential theory.

the valley center [Fig. 2(b)]. Near the ridge center, the emission intensity of transition B decreases to zero. Line scans perpendicular to the ridge [Fig. 2(c), filled circles] highlight the spatial anticorrelation of the two emission components A and B. This demonstrates the existence of two spatially and spectrally distinct optical transitions in our sample and gives direct evidence for a strain-induced lateral carrier confinement in the InGaAs QW. A detailed analysis of the near-field PL spectra indicates that the local near-field luminescence spectra $PL(E_{\text{det}}, x, y)$ are well described by a weighted sum of the two emission spectra $A(E_{\text{det}})$ and $B(E_{\text{det}})$ [Fig. 2(d)] with space-dependent weighting coefficients similar to those shown in Figs. 2(a) and 2(b). The slight spatial fluctuations of luminescence intensity along the ridge direction, therefore, reflect local changes in the luminescence efficiency rather than spatial fluctuations of the emission spectra, as observed in quantum wells showing pronounced exciton localization under similar excitation conditions.¹¹ The absence of spectrally sharp emission resonances from localized excitons in the present samples is attributed to the short scale fluctuations of the alloy composition in the InGaP stressor layers discussed above.

FEM calculations⁹ were performed in order to analyze the role of patterning induced strain distribution on this lateral confinement potential. These calculations indicate that the relaxation of the InGaP lattice parameter near the {111} grating side facets creates an additional compressively strained region beneath the valley. In general, compressive strain causes a blueshift of the emission from InGaAs. The lateral shifts of conduction- and valence-band edges (x , along the grating repetition direction) were calculated using the local strain tensor obtained by FEM calculations in a deformation potential ansatz^{3,12,13} (Fig. 3). The impact of strain on the conduction band edge is more pronounced than on the valence-band edge. Thus, the strain influence on the optical properties can mainly be estimated from the shift of the conduction band. A band-edge shift of about 28 meV is obtained in the regions of maximum compressive strain located at the edges of the valleys. Inside the valley, the conduction-band edge decreases in energy, but it is still higher than for the

initial (unpatterned) structure. Beneath the ridge the conduction-band edge is slightly lower compared to the initial value. If electron-hole pairs are excited in such a structure, the carriers can diffuse freely only along the [1-10] direction, while the potential barrier near the valley edges hinders diffusion along the grating direction. Thus, electrons excited beneath the ridge are laterally confined due to the conduction-band potential barriers near the valley corners. These barriers also confine electrons beneath the valleys due to the band-edge difference of about 15 meV between the edges and the middle of the valley. Since a weaker barrier also exists in the valence band, electron-hole recombination is expected either at the center of the valley or beneath the ridge. Thus, two spatially and spectrally distinct electronic transitions are expected to originate from the region beneath the ridges and the region beneath the valleys, respectively. These theoretical predictions are in excellent agreement with the experimentally observed spatial anticorrelation of peaks A and B, spectrally separated by about 10 meV and located under the grating ridges and valleys, respectively.

In conclusion, we have demonstrated an approach for lateral band-gap modulation of an InGaAs single quantum well by a patterned InGaP stressor layer. Strain relaxation at the facets of a lateral surface grating gives rise to spatially and spectrally distinct optical transitions and lateral carrier confinement with a confinement energy of about 10 meV. This is in accordance with FEM simulations of the strain distribution within the sample and directly evidenced by low-temperature near-field photoluminescence spectroscopy.

The authors gratefully acknowledge the financial support of the work by Deutsche Forschungsgemeinschaft under Contract Nos. Tr 357 and Pi 217, by Contract No. SFB 296 and the European Union through the EFRE program, and the TMR Network Ultrafast Quantum Optoelectronics for one of the authors (G.C.), and a Marie Curie Fellowship (ERB4001GT975127) for one of the authors (V.E.). The authors thank A. Klein for the transmission electron microscopy investigations.

¹Y. Arakawa and H. Sakaki, Appl. Phys. Lett. **40**, 939 (1982).

²F. Klopff, J. P. Reithmayer, and A. Forchel, Appl. Phys. Lett. **77**, 1419 (2000).

³D. Bimberg, M. Grundmann, and N. N. Ledentsov, *Quantum Dot Heterostructures* (Wiley, Chichester, 1998).

⁴B. P. Van der Gaag and A. Scherer, Appl. Phys. Lett. **56**, 481 (1990).

⁵A. Forchel, R. Steffen, T. Koch, M. Michel, M. Albrecht, and T. L. Reinecke, Semicond. Sci. Technol. **11**, 1529 (1996).

⁶K. Kash, J. M. Worlock, D. M. Sturge, P. Grabbe, J. P. Harbinson, A. Scherer, and P. S. D. Lin, Appl. Phys. Lett. **53**, 782 (1988).

⁷K. Kash, B. P. Van der Gaag, D. D. Mahoney, A. S. Gozdz, L. T. Florez, J. P. Harbinson, and M. D. Sturge, Phys. Rev. Lett. **67**, 1326 (1991).

⁸M. Sopranen, H. Lipsanen, and J. Ahopelto, Appl. Phys. Lett. **66**, 2364 (1995).

⁹U. Zeimer, J. Grenzer, U. Pietsch, S. Gamlich, F. Bugge, V. Smirnitki, M. Weyers, and G. Tränkle, J. Phys. D **34**, A183 (2001).

¹⁰G. Behme, A. Richter, M. Süptitz, and Ch. Lienau, Rev. Sci. Instrum. **68**, 3458 (1997).

¹¹F. Intonti, V. Emiliani, Ch. Lienau, T. Elsaesser, R. Nötzel, and K. H. Ploog, Phys. Rev. B **63**, 075313 (2001).

¹²G. Bir and G. Pikus, *Symmetry and Strain-Induced Effects in Semiconductors* (Wiley, Chichester, 1974).

¹³U. Pietsch, N. Darowski, A. Ulyanenkov, J. Grenzer, K. H. Wang, and A. Forchel, Physica B **283**, 92 (2000).